Soot growth by monodisperse particle dynamics model coupled with Computational Fluid Dynamics

Arash Fakharnezhad [1], Joseph D. Berry[1], Eirini Goudeli [1]

[1] Department of Chemical Engineering, The University of Melbourne, Parkville, Melbourne VIC 3010, Australia

5   *Correspondence to*: Eirini Goudeli (eirini.goudeli@unimelb.edu.au)

Abstract. A multiscale modeling framework, integrating molecular dynamics (MD)-derived soot nucleation and surface growth rates into a coupled computational fluid dynamics (CFD)-monodisperse particle dynamics (PD) model, is implemented and benchmarked for a premixed ethylene burner-stabilized stagnation (BSS) flame. The proposed coupled model is validated by comparing the soot number density, volume fraction, and particle size with measurements across the BSS flame, as well as

10   with the results obtained by CFD-PD using a semi-empirical nucleation rate by Moss-Brookes and the Hydrogen Abstraction Carbon Addition (HACA) surface growth rate. Incorporation of the MD-derived nucleation rate is in excellent agreement with both experimental data and a detailed sectional model from the literature, especially in the post-flame region. The proposed MD-informed CFD-PD model is computationally efficient compared to detailed population balance equation models as it does not rely on reaction kinetic modeling and can serve as a predictive tool for soot modeling and design-oriented simulations of

15   practical combustion and aerosol systems.

1 Introduction

Soot formation in combustors and flames is inherently multiscale, involving coupled chemical and physical processes (Michelsen, 2017) that span several orders of magnitude in length and time. At the molecular zone, soot formation begins with reactions of small radicals and hydrocarbon fragments, only a few Angstroms in size, that form polycyclic aromatic

20   hydrocarbons (PAHs), the main precursors of soot (Frenklach, 2002) as shown by atomic force microscopy (Schulz et al., 2019). These PAHs evolve into sub-2 nm soot nuclei through physical or chemical nucleation, which grow by surface reactions into primary particles (Mitchell and Frenklach, 2003). The primary particles coagulate by aggregation and/or agglomeration to form large (>100 nm) aggregates within micro- to milliseconds (Michelsen, 2017). Reactive flow in combustors and flames extends over dimensions on the order of meters and particle residence times on the order of seconds, which strongly influence

25   soot evolution (Trivanovic and Pratsinis, 2024; Kelesidis et al., 2017).

Hierarchical modeling provides a pathway to address the multiscale nature of soot formation and growth by linking information across different length and time scales (Goudeli, 2019). Molecular dynamics (MD) simulations can capture the onset and early stages of soot nucleation (Mao et al., 2017), as well as surface growth (Chen and Luo, 2020) and coalescence (Sharma et al., 2021), but remain limited to a few nanometers and hundreds of nanoseconds. Traditionally, soot nucleation has

30   been modeled using physical PAH-PAH interactions, such as the POLIMI soot nucleation sub-model (Saggese et al., 2015), whereas more recent approaches adopt hybrid (physical-chemical) reactive PAH dimerization models (Kholghy et al., 2018). More recently, reactive Molecular Dynamics (MD) has been employed to determine the critical nucleus size and nucleation rate of carbonaceous nanoparticles (Fakharnezhad et al., 2025). Particle-scale models, such as event-driven simulations (Patterson and Kraft, 2007; Goudeli et al., 2015; Kelesidis et al., 2017) can resolve particle interactions, while continuum

35   models, such as population balance equations and Computational Fluid Dynamics (CFD) can track particle growth and transport (Saggese et al., 2016), respectively, reaching length and time scales of micrometers and seconds. For example, event-driven mesoscale simulations of soot nanoparticles have been used to determine the coagulation rate in the transition regime, yielding an enhancement of 82% over the harmonic mean interpolation between the theoretical kernels of the free molecular and continuum regime (Kelesidis and Goudeli, 2021). Such corrections have been implemented into monodisperse particle

40   dynamics simulations (Fakharnezhad et al., 2026) to account for the primary particle and aggregate polydispersity. A similar hierarchical modeling framework has been also applied for TiO_2 nanoparticle synthesis, where fractal dimension and coagulation rate equations derived from Langevin dynamics (Chen et al., 2023) were incorporated into a CFD-PBM model (Chen et al., 2023), along with sintering rates obtained by MD simulations (Buesser et al., 2011), linking molecular-, particle- and continuum-scale simulations.

45   The evolution of soot particle population can be described by the General Dynamic Equation, a partial integro-differential equation, requiring the implementation of numerical methods. One highly accurate numerical approach relies on the sectional method, where the particle population is divided into size bins and transport equations are solved for each class (Saggese et al., 2015), but its computational cost increases with the number of sections, making it impractical for multidimensional CFD simulations (Saggese et al., 2016; Kholghy and Kelesidis, 2021). A computationally less demanding

50   alternative is the method of moments (MOM) (Hulburt and Katz, 1964), which tracks only a few statistical moments of the distribution (e.g., number, mass, surface area). However, MOM relies on closure assumptions (Kholghy and Kelesidis, 2021), limiting accuracy when soot distributions deviate from the assumed shape.

        The particle dynamics equation can be greatly simplified when assuming monodisperse particles or aggregates at a given location (Kruis et al., 1993). So, the soot population can be represented by a single average size, requiring tracking the

55   evolution of only the number density, surface area, and volume (Kholghy and Kelesidis, 2021). Even though PD neglect the spread of soot size distribution, this simplification typically results in deviations of up to 30 % (Kholghy and Kelesidis, 2021) in the predicted evolution of soot volume fraction, number density, and average particle diameters compared to polydisperse population balance equations, owing to the rapid attainment of the self-preserving size distribution (Kholghy and Kelesidis, 2021) and an asymptotic collision frequency function therein, regardless of the primary particle polydispersity (Goudeli et al.,

60   2016). Therefore, monodisperse PD models can provide average aggregate characteristics reasonably well at a much lower computational cost than sectional methods or MOM, making them attractive for coupling with multidimensional CFD simulations in realistic geometries.

Another challenge in soot kinetic models, such as POLIMI (Saggese et al., 2015), is that nucleation and surface growth rates are derived directly from detailed gas-phase chemistry. For example, nucleation is typically described through PAH-PAH interactions, which requires prior calculation of PAH concentrations using large kinetic mechanisms that involve many species and reactions (Ranzi et al., 2012). Similarly, surface growth is governed by detailed chemistry, proceeding either through radical-driven pathways or via condensation of PAHs and their fragments onto soot particles (Saggese et al., 2015). As such, both pathways are tied to extensive gas-phase mechanisms, which can be computationally prohibitive for multidimensional CFD simulations in realistic geometries. Traditionally, however, soot formation was described using semi-empirical models, in which nucleation and surface growth were correlated directly to acetylene rather than PAH concentrations (Brookes and Moss, 1999). While far more efficient and straightforward to implement, these correlations were developed for specific flame conditions and lack generalizability across different fuels and operating conditions (Johnson et al., 2021; Fakharnezhad et al., 2026). Thus, both detailed PAH-based and semi-empirical acetylene-based models face critical limitations when applied to practical design applications.

Here, lumped, acetylene concentration-dependent nucleation (Fakharnezhad et al., 2026) and surface growth (Goudeli et al., 2025) rates derived from reactive MD are implemented into an easy-to-use monodisperse PD model (Fakharnezhad et al., 2026), which accounts for simultaneous nucleation, surface growth and coagulation. The PD model is coupled with two-dimensional CFD to account for the flame geometry and fluid flow. These MD-derived rates, obtained without assumptions about the contributing reaction pathways or precursor species (Fakharnezhad et al., 2025), do not require simultaneous implementation or use of detailed gas-phase reaction mechanisms. The performance of these MD-derived rates is systematically assessed against established nucleation and surface growth rates from the literature implemented in the developed CFD-monodisperse framework, and the results are benchmarked against a detailed sectional model (Saggese et al., 2015; Saggese et al., 2016) and experiments from a burner-stabilized stagnation (BSS) flame (Camacho et al., 2015). The results are also compared to those obtained from the standard semi-empirical Moss-Brookes model for spherical soot nanoparticles implemented in Fluent, which is also based on a monodisperse particle dynamics formulation but assumes coagulation only by full coalescence.

2 Theory

2.1 CFD model

ANSYS Fluent (V 2023 R1) was applied to model soot formation in a BSS laminar flame (Camacho et al., 2015). This flame was chosen for its well-defined flame geometry consisting of a porous plug burner, featuring nitrogen shielding for isolation from ambient air, and an adjustable cooled stagnation plate with an embedded orifice, facing the incoming flow for sampling (Camacho et al., 2015), with dimensions provided in Fig. 1.

The flow geometry is axisymmetric, so the velocity, temperature, and species composition depend solely on the axial and radial directions. Consequently, the computational domain is reduced to a two-dimensional rectangular section,

95   representing a radial-axial slice (Fig. 1: side 6), which is revolved around the axis of symmetry to model the full cylindrical flame geometry. This 2D domain was discretized into 46,400 quadrilateral cells using a non-uniform mesh. The cell size ranges from ~0.05 mm in the axial direction near the reactant inlet and stagnation plate up to 0.2 mm away from them.

     The Navier-Stokes equations were solved at steady state using a pressure-based solver that ensures mass conservation through a pressure correction equation. The energy equation was also included to capture thermal variations, and a laminar

100   flow model was applied to describe viscous effects. Species transport was modeled using the Volumetric Reaction approach (Kee et al., 2005) with the DRM22 reaction mechanism (Kazakov and Frenklach, 1995), including 22 species and 104 reactions. The DRM22 was developed as a reduced form of GRI-Mech 1.2 and has been validated against detailed mechanism predictions of ignition delays and laminar premixed methane-air flame properties over a wide range of conditions, showing deviations typically below 5% (Kazakov and Frenklach, 1995). This mechanism is further validated here, as discussed in

105   Section 3.1.1**Error! Reference source not found.**. The CHEMKIN-CFD chemistry solver was employed including thermal d iffusion effects.
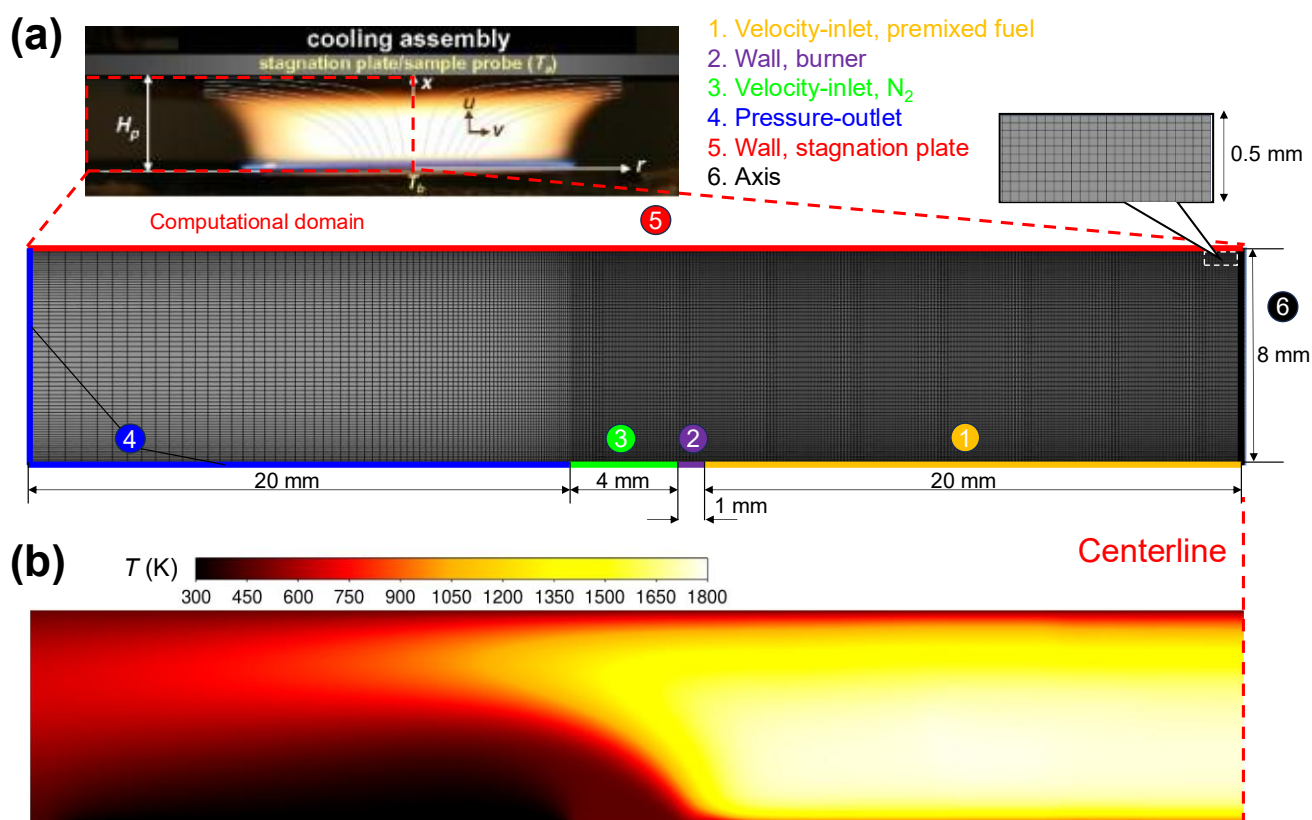

Figure 1: (a) Schematic of the computational domain with applied boundary conditions, and mesh configuration used in the CFD simulation, along with (b) a representative contour plot of the resulting temperature field.

110

2.2 Boundary Conditions

At the premixed inlet, the velocity components, temperature, and species mass fluxes are prescribed. The axial velocity is set to $v = 0.14$ m/s and the temperature is fixed at $T = 473$ K (Saggese et al., 2016). The species fluxes account for both convective and diffusive contributions, ensuring mass conservation at the boundary:

$$\rho v Y_k + \rho Y_k V_k = (\rho v Y_k)_{z=0} \tag{1}$$

where ρ is the gas density, Y_k is the mass fraction of species k, and V_k is the diffusion velocity. The species balance fluxes that account for both convective and diffusive contributions were obtained from Chemkin-Pro at identical conditions and were imposed as the inlet boundary condition in the Fluent solver (see Appendix). A pure nitrogen inlet is defined with inlet velocity of 0.4 m/s and temperature of 473 K (Saggese et al., 2016). The stagnation surface is treated as a no-slip wall with a fixed temperature of 500 K (Saggese et al., 2016). At the outlet, an atmospheric pressure condition is applied, allowing the flow to exit the domain naturally.

2.3 Soot dynamics

The evolution of soot was described using a monodisperse PD framework coupled to the CFD solver in ANSYS Fluent through user-defined functions. Specifically, the evolution of total particle number density N and the carbon molar concentration C was modelled using CFD transport equations, with nucleation, surface growth, and coagulation rates incorporated as custom source terms through user-defined functions in Fluent. In this implementation, the transport of total particle number density N is described by:

$$\frac{\partial(\rho u_i N)}{\partial x_i} - \frac{\partial}{\partial x_i}\left(\Gamma_{k,N}\frac{\partial N}{\partial x_i}\right) = \left(\frac{dN}{dt}\right)^{Nucl.} + \left(\frac{dN}{dt}\right)^{Coag.} \tag{2}$$

and the transport of carbon molar concentration C is defined by:

$$\frac{\partial(\rho u_i C)}{\partial x_i} - \frac{\partial}{\partial x_i}\left(\Gamma_{k,C}\frac{\partial C}{\partial x_i}\right) = \left(\frac{dC}{dt}\right)^{Nucl.} + \left(\frac{dC}{dt}\right)^{SG} \tag{3}$$

The terms on the left-hand side of equations (2) and (3) represent convection and diffusion in the flow, where u_i denotes the velocity, and $\Gamma_{k,N}$ and $\Gamma_{k,C}$ are the effective diffusion coefficients for number density and carbon concentration, respectively. The right-hand side of eq. (2) includes the nucleation term, which describes the formation of new particles, and the coagulation term, which describes the reduction in the number of particles due to agglomeration. In eq. (3), the source terms correspond to carbon addition due to newly formed particles by nucleation, and carbon accumulation on existing particles due to surface growth.

The total soot surface area concentration, A, is not explicitly solved in this implementation. Instead, it is reconstructed from N and C using a morphological relationship (Xiong and Pratsinis, 1993):

$$\frac{A/N}{a_0} = \left(\frac{V/N}{v_0}\right)^{D_s/3} \tag{4}$$

140   where a_0 and v_0 denote the surface area and volume of a primary soot particle, $V = \frac{C\,MW_C}{\rho_{soot}}$ is the total soot volume

concentration of the whole particle population, and D_s is the surface fractal dimension. For spherical particles, $D_s = 2$, while

for agglomerates and aggregates D_s spans between 2 and 3. The D_s correlation along with the coagulation kernel employed in

this study, are detailed in (Fakharnezhad et al., 2026).

       The source terms for nucleation and surface growth follow established literature models in the baseline framework

145 (as listed in Table 1), where the Moss-Brookes acetylene-based nucleation rate (Brookes and Moss, 1999) is combined with

the Hydrogen Abstraction Carbon Addition (HACA) surface growth mechanism (Appel et al., 2000) (Model I). To assess the

impact of molecular-level rate expressions, three additional cases were considered: in Model II, the Moss-Brookes nucleation

rate was replaced with the MD-derived nucleation rate (Fakharnezhad et al., 2026) while keeping HACA unchanged; in Model

III, nucleation is described by the Moss-Brookes equation while surface growth was substituted with a MD-derived rate

150 (Goudeli et al., 2025); and in Model IV, both nucleation and surface growth were described using MD-derived expressions.

For comparison, the Moss-Brookes soot model (Brookes and Moss, 1999) implemented in Fluent (Model V) is also considered,

as it is widely used in design applications. The latter is a semi-empirical, monodisperse formulation coupled with CFD,

assuming full coalescence of spherical particles during coagulation in the free-molecular regime. Additionally, a detailed

sectional CFD-PBE model from the literature (Saggese et al., 2015; Saggese et al., 2016) (Model VI) is included, representing

155 1-D and 2-D simulations with full gas-phase chemistry and soot dynamics. The results of this model reported in the literature

(Saggese et al., 2015; Saggese et al., 2016) are used to benchmark the proposed reduced framework against detailed sectional

simulations. Overall, these six models (see Table 1) encompass a range of physical assumptions and are systematically

benchmarked against experiments in Section 3.

3 Results and discussion

160 ### 3.1 Validation

3.1.1 Reaction mechanism

The reduced DRM22 mechanism (Kazakov and Frenklach, 1995) was first benchmarked in one-dimensional Chemkin-Pro

simulations against a well-characterized premixed ethylene flame ($\Phi \approx 1.7$) (Gerasimov et al., 2012), where detailed

experimental measurements are available, providing a suitable reference for validation under conditions comparable to the

165 flame under investigation. Figure 2 shows the mole fraction profiles of major and intermediate species as a function of the

height above the burner (HAB), including (a) H_2O, H_2, O_2, (b) CO, CO_2, C_2H_4, and (c) C_2H_2, CH_4. The predictions are in

excellent agreement with measurements (Gerasimov et al., 2012) of O_2 and C_2H_4 consumption and H_2O, CO, H_2, and CO_2

formation (Fig. 2a and b), validating the employed chemical reaction scheme for oxidation. The mechanism also captures the trend and order of magnitude of the mole fraction of C$_2$H$_2$ and CH$_4$ intermediates (Fig. 2c), validating further the DRM22

170   mechanism for the chemistry of the present premixed ethylene flame.

Table 1: Summary of soot nucleation and surface growth models employed in this study.

| Soot Model	Nucleation rate		Surface Growth (SG) rate		Modeling framework	Remarks	Reference
	Model	Rate expression	Model	Rate expression			
I	Moss-Brookes	$C_\alpha N_{Av} \exp\left(-\frac{T_\alpha}{T}\right)[C_2H_2]$	HACA	$2k_s \alpha \chi_{soot-H} \frac{k_f}{k_b} \frac{[H]}{[H_2]}[C_2H_2] \frac{A}{N_{Av}}$	CFD-monodisperse PD (this work)	Implemented as discussed in Section 2.3.	Nucleation rate: (Brookes and Moss, 1999) SG rate: (Appel et al., 2000)
II	MD-derived	$k_{MD}[C_2H_2]^{3.5}$	HACA	$2k_s \alpha \chi_{soot-H} \frac{k_f}{k_b} \frac{[H]}{[H_2]}[C_2H_2] \frac{A}{N_{Av}}$			Nucleation rate: (Fakharnezhad et al., 2026) SG rate: (Appel et al., 2000)
III	Moss-Brookes	$C_\alpha N_{Av} \exp\left(-\frac{T_\alpha}{T}\right)[C_2H_2]$	MD-derived	$k_{MD,SG} \frac{k_f}{k_b} \frac{[H]}{[H_2]}[C_2H_2]A$			Nucleation rate: (Brookes and Moss, 1999) SG rate: (Goudeli et al., 2025)
IV	MD-derived	$k_{MD}[C_2H_2]^{3.5}$	MD-derived	$k_{MD,SG} \frac{k_f}{k_b} \frac{[H]}{[H_2]}[C_2H_2]A$			Nucleation rate: (Fakharnezhad et al., 2026) SG rate: (Goudeli et al., 2025)
V	Moss-Brookes	$C_\alpha N_{Av} \exp\left(-\frac{T_\alpha}{T}\right)[C_2H_2]$	Moss-Brookes	$C_\gamma [C_2H_2] \exp\left(-\frac{T_\gamma}{T}\right)\left[(\pi N)^{1/3}\left(\frac{6M}{\rho_{soot}}\right)^{2/3}\right]$	CFD-monodisperse PD as implemented in Fluent	Moss-Brookes soot model, assuming full coalescence in the free-molecular regime.	(Brookes and Moss, 1999)
VI	PAH-PAH interactions	$AT^n \exp\left(-\frac{E}{RT}\right)[PAH]^2$	HACA + RR addition + PAH addition		CFD-sectional PBE model	Detailed 1D and 2D simulations with full gas-phase chemistry and soot dynamics.	(Saggese et al., 2015; Saggese et al., 2016)

7
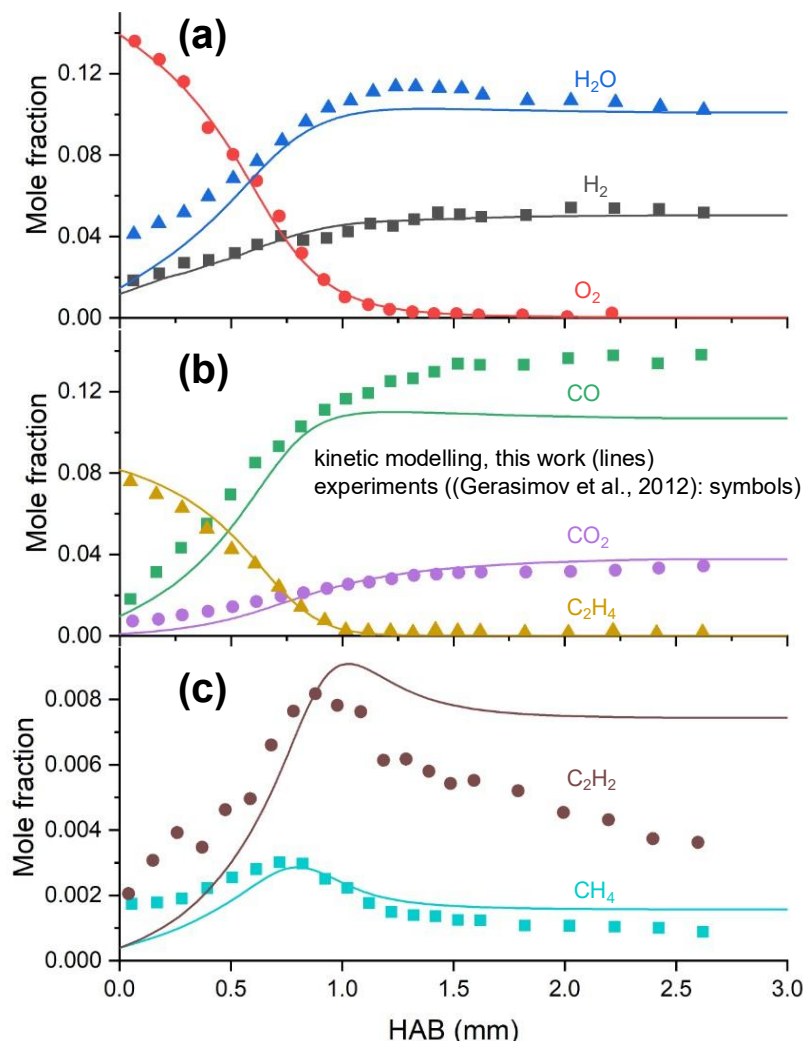
Figure 2: Species profiles as a function of the height above the burner, HAB, in the premixed $C_2H_4/O_2/Ar$ sooting flame (equivalence ratio, $\Phi = 1.7$) obtained by experiments ((Gerasimov et al., 2012): symbols) and kinetic modeling (lines).

3.1.2 Computational Fluid Dynamics (CFD) Model

Figure 3 shows the CFD-predicted centerline temperature profile (line) as a function of HAB, showing excellent agreement with temperature measurements in BSS flames (Camacho et al., 2015): symbols). The temperature increases abruptly with HAB up to 1 mm, and reaches a maximum of approximately 1700 K between HAB = 1–4 mm, before it drops downstream in the flame (HAB > 4 mm) as it approaches the stagnation plate at HAB = 8 mm. The CFD-obtained temperature contour (Fig. 1b) also nicely reproduces the overall shape of the real flame by experiments (Fig. 1a), confirming that the thermal field is described reliably.
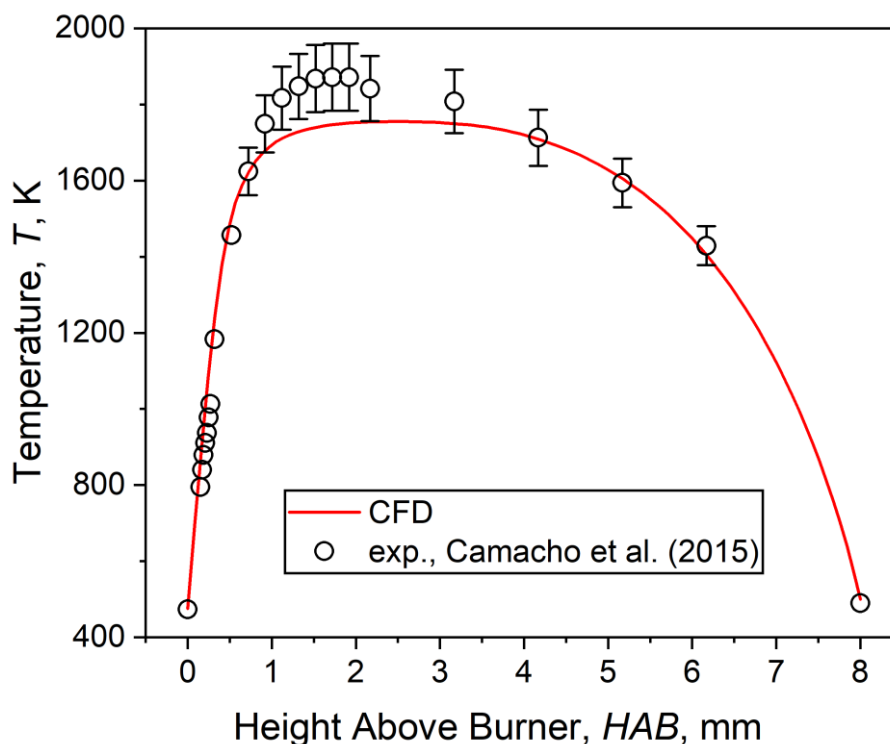
Figure 3: Centreline temperature profile as a function of HAB obtained by CFD (line) and experiments (Camacho et al., 2015).

3.2 Soot growth by coupled CFD-PD simulations

The coupled CFD-PD model (eqs. 2–4) tracks the soot number density, carbon concentration, and surface area evolution accounting for nucleation, surface growth, and coagulation, as described in Section 2.3. Figure 4 shows contours of the soot number density, N (Fig. 4a), and volume fraction, f_v (Fig. 4b), in the sooting flame for burner-to-stagnation plate separation, H_p, of 8 mm, obtained using the Moss-Brookes nucleation rate and HACA surface growth rate (Model I: baseline model). Although a 2D axisymmetric domain was used, the analysis focuses on the flame centerline, consistent with the 1D approximation of BSS flames (Saggese et al., 2016). Near the burner exit (HAB = 0–1 mm), where the temperature of fresh premixed gas starts to increase as it combusts and intermediate species (such as C_2H_2) form, limited soot nucleation may occur. However, the soot precursors still form and nucleation is not yet dominant. Downstream in the flame, at HAB = 1–5 mm, the temperature reaches its maximum, and ethylene decomposes to acetylene and other soot precursors that result in pronounced nucleation and subsequent particle growth.
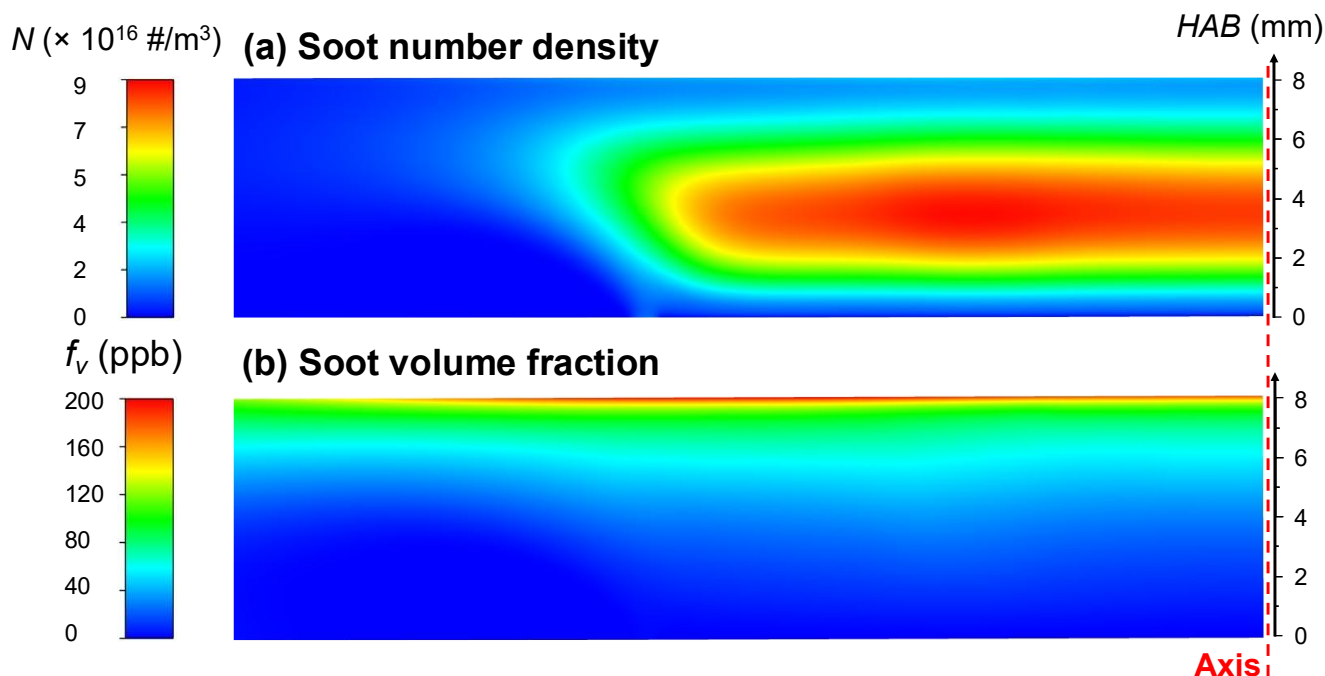
9

Figure 4: Contours of soot (a) number density, N, and (b) volume fraction, f_v, in the sooting flame with burner-to-stagnation plate separation of H_p = 8 mm (predicted using Model I: Moss-Brookes nucleation and HACA surface growth rates).

The soot number density increases rapidly after the onset of nucleation, reaching a maximum of $N = 9 \times 10^{16}$ #/cm³ at HAB ≈ 3.6 mm, while at HAB > 3.6 mm it decreases as coagulation takes over (Fig. 4a). In contrast, the soot volume fraction increases continuously downstream in the flame as particle mass grows through reactions of gaseous reactive species with the soot particle surface, even though their number density decreases by coagulation. The highest soot loading is observed close to the stagnation plate (Fig. 4b). Since the probe was positioned along the centreline but not explicitly included in the 2D simulation, its effect was accounted for by shifting the sampling position upstream along the axial direction following the correction of Saggese et al. (Saggese et al., 2016). The required spatial shift ranges from 1 to 1.6 mm, depending on the burner-to-plate separation, as obtained from the probe-effect analysis (Saggese et al., 2016). For this case, the highest soot loading is ~100 ppm after applying a 1.5 mm shift. This correction was applied to all results to ensure consistency with experiments.

Figure 5 shows the soot number density and soot volume fraction predicted by the CFD-coupled monodisperse PD model using different nucleation and surface growth rates (Table 1: Models I-IV) as well as by the Moss-Brookes soot model implemented in Fluent (Model V) at probe locations, H_p, of 8 mm and 4 mm above the burner. The results are compared to a 2D CFD-Sectional PBE model by Saggese et al. (Saggese et al., 2016) Table 1: Model VI), who reported N and f_v in these two probe locations, and to experiments (Camacho et al., 2015) at the same H_p of the BSS ethylene flame.
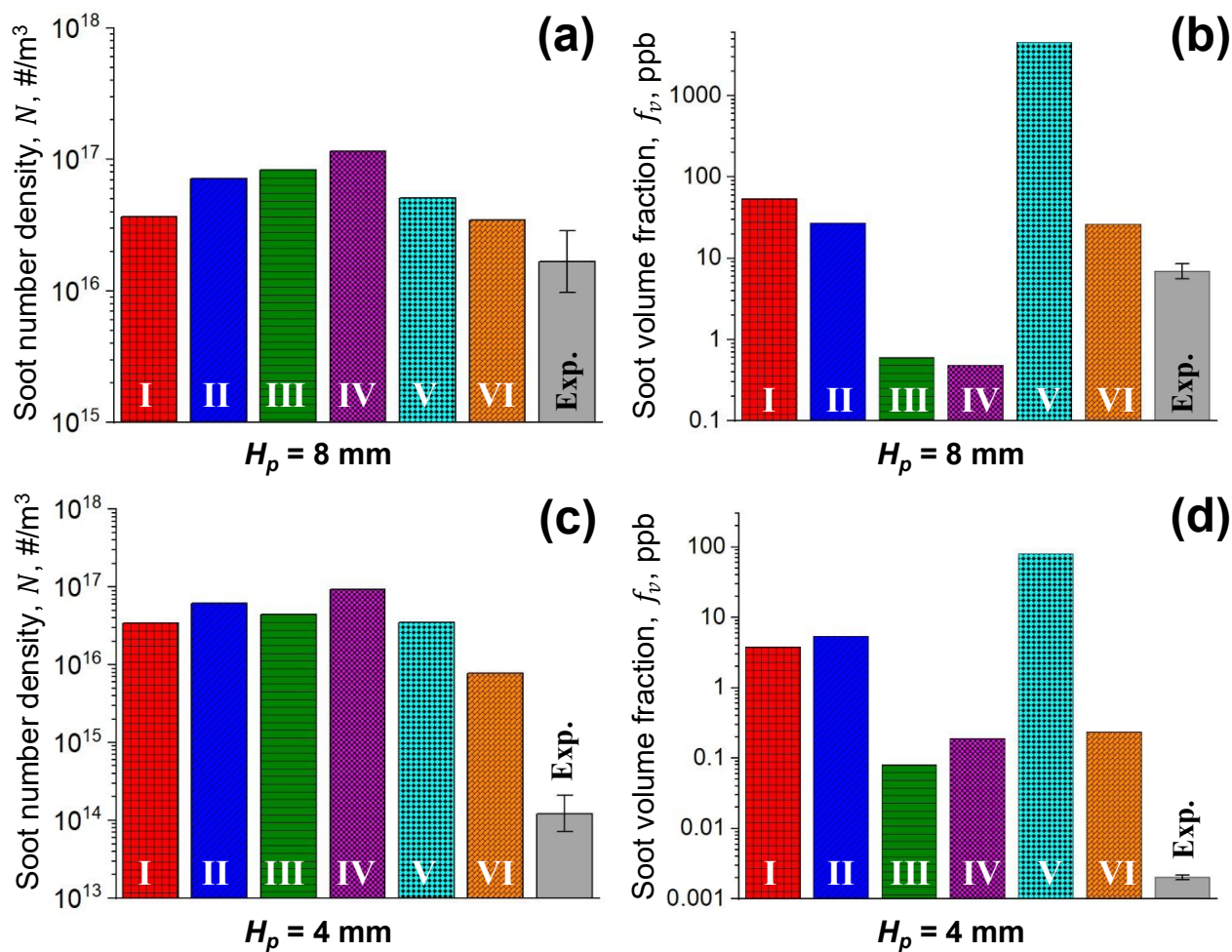
Figure 5: (a, c) Soot number density (N) and (b, d) volume fraction (f_v) at (a, b) H_p = 8 and (c, d) 4 mm obtained by CFD-coupled monodisperse PD with various nucleation and surface growth rates (models I to IV) and by the Moss-Brookes soot model implemented in Fluent (Model V). The results are compared to a 2D sectional model (Saggese et al., 2016): Model VI) and experiments (Camacho et al., 2015) in the same BSS ethylene flame.

At H_p = 8 mm (Fig. 5a), the CFD-coupled monodisperse PD model with the Moss-Brookes nucleation rate and HACA surface growth rate (Model I, baseline) yields $N = 3.66 \times 10^{16}$ #/cm³, overpredicting the experimental value of 1.66×10^{16} #/cm³. However, the prediction is comparable (within ~6%) to that reported by Saggese et al. (Saggese et al., 2016) (Model VI; $N = 3.44 \times 10^{16}$ #/cm³). Replacing the nucleation and/or surface growth rates with the MD-derived expressions (Models II–IV) results in higher N values (up to about a factor of three) relative to Model I, while the differences among all models, including Model V, remain within the experimental uncertainty at this H_p.

The baseline model (Model I) predicts f_v= 54 ppb (Fig. 5b), which is about twice that obtained from the sectional model

230   (Model VI; f_v= 26.1 ppb (Saggese et al., 2016)) but within one order of magnitude of the measured f_v of 7 ppb. This indicates

that the present framework reproduces soot mass loading with an accuracy comparable to that of detailed sectional modeling.

When nucleation is described by the MD-derived rate (Model II), f_v decreases down to 28.4 ppb, matching the sectional model

prediction within ~4 % and improving agreement with the measured f_v by ~57 % compared to Model I. Accounting for the

MD-derived surface growth rate (Models III and IV) decreases the f_v down to 5.7 (Model III) and 3.8 ppb (Model IV), below

235   the measured soot mass loading. The underprediction of f_v in Models III and IV, which incorporate the MD-derived surface

growth rate, can be attributed to their substantially lower surface growth contribution compared to the baseline model using

the HACA mechanism. The carbon addition rate from surface growth, $\left(\frac{dC}{dt}\right)^{SG}$, in these models is almost two orders of

magnitude lower than in Model I (Fig. S1), especially across the main soot-forming region (1–7 mm). This reduction in carbon

addition explains the lower soot mass predicted by the MD-derived surface growth models.

240   The Moss-Brookes soot model (Model V) yields $N = 5.11 \times 10^{16}$ #/cm³ (Fig. 5a), which is comparable to all the other

models (Models I–IV) considered, yet the corresponding f_v (4,572 ppb) is nearly three orders of magnitude higher than the

measured f_v and the highest among all models. This overprediction stems from the excessive surface growth contribution (Fig.

S1), which is nearly three orders of magnitude larger than in the baseline case. These results confirm that surface growth

dominates soot mass formation and strongly influences f_v predictions, consistent with the literature (Harris and Weiner, 1985).

245   At H_p = 4 mm (Fig. 5c,d), the baseline model yields $N = 3.44 \times 10^{16}$ #/cm³ and f_v = 3.43 ppb, about one order of

magnitude higher than those obtained by the sectional model ($N = 7.82 \times 10^{15}$ #/cm³ and f_v = 0.24 ppb), and two and three

order of magnitude higher than the experimentally measured N of 1.22×10^{14} #/cm³ and f_v of 0.002 ppb. Models II to V show

comparable trends for both soot number density and volume fraction, as also observed at H_p = 8 mm (Fig. 5a,b). Overall, all

models substantially overpredict the experimental data at H_p = 4 mm, with deviations of approximately two to three orders of

250   magnitude for both N and f_v.

The performance of the proposed model is assessed across a broader range of burner-to-stagnation plate separations

investigated experimentally, as shown in Fig. 6. The results are compared against the 1D sectional model of Saggese et al.

(Saggese et al., 2015), which employed the same soot sub-model as the 2D simulations and covered H_p values from 4 to 12

mm. Figure 6 shows (a) the soot number density and (b) soot volume fraction as a function of H_p, as predicted by Models I–

255   V, the 1D sectional model (Model VI: (Saggese et al., 2015), and experiments (Camacho et al., 2015). The soot number density

predicted by Models II-V is practically constant across all H_p. Model I suggests a slight decrease in the soot number

concentration with H_p, which is qualitatively consistent with the detail sectional model and in reasonable agreement with

measurements (circles) for $H_p \geq 6$ mm. At H_p = 4 mm, however, all models overpredict N by 2–3 orders of magnitude. This

discrepancy has been partially attributed to simplifications made in employed nucleation mechanisms (Hou et al., 2019), even

260   though it may also stem from the presence of sub-2 nm soot nuclei (Fakharnezhad et al., 2026) undetected during measurements
by standard butanol- or water-based condensation particle counters (Camacho et al., 2015).

Even though all models suggest soot number concentrations comparable to each other (within one order of
magnitude), they result in distinct soot volume fractions that span over up to 5 orders of magnitude (Fig. 6b). Both Models I
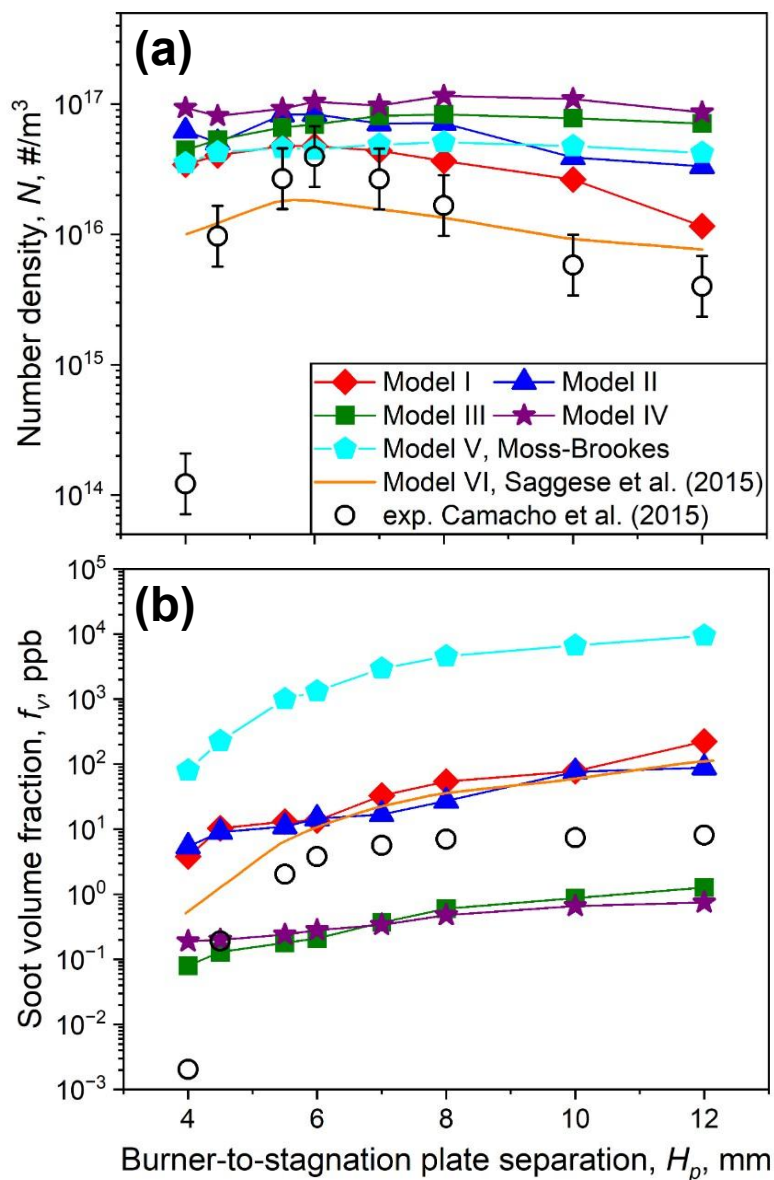
Figure 6: (a) Soot number density, N, and **(b)** volume fraction, f_v, as a function of H_p as obtained by CFD-coupled monodisperse
PD with various nucleation and surface growth rates (models I to IV) and by the Moss-Brookes soot model implemented in Fluent
(Model V) (filled symbols). The results are compared to 1D sectional model (Model VI) reported in line) and soot measurements
(circles) in ethylene premixed flames (Camacho et al., 2015). The error bars for the measured f_v (not shown) are within the
symbol size.

270   and II yield comparable f_v predictions, in good agreement with the sectional model (Saggese et al., 2015) and measurements (Camacho et al., 2015) within up to one order of magnitude for $H_p \geq 6$ mm. In contrast, the Moss-Brookes soot model (Model V) overpredicts the soot volume fraction by nearly three orders of magnitude, whereas Models III and IV underpredict the measurements by about two orders of magnitude. As previously shown at $H_p = 8$ mm (Fig S1), this underprediction is caused by the lower carbon addition rate from surface growth, which primarily arises from the fact that the MD-derived effective

275   surface growth rate constant (Goudeli et al., 2025) is approximately three times lower than that predicted by the HACA-based correlation of Appel et al. (Appel et al., 2000). This slower surface growth rate limits carbon accumulation in the soot phase resulting in lower soot volume fractions. At $H_p = 4$ mm, all reduced models overpredict the measurements by 2–5 orders of magnitude. Such a significant overprediction is not unique to the low-order modeling framework (Models I-V), as it is observed even with detailed sectional models (Model VI), which had been attributed to incomplete description of soot nucleation PAH

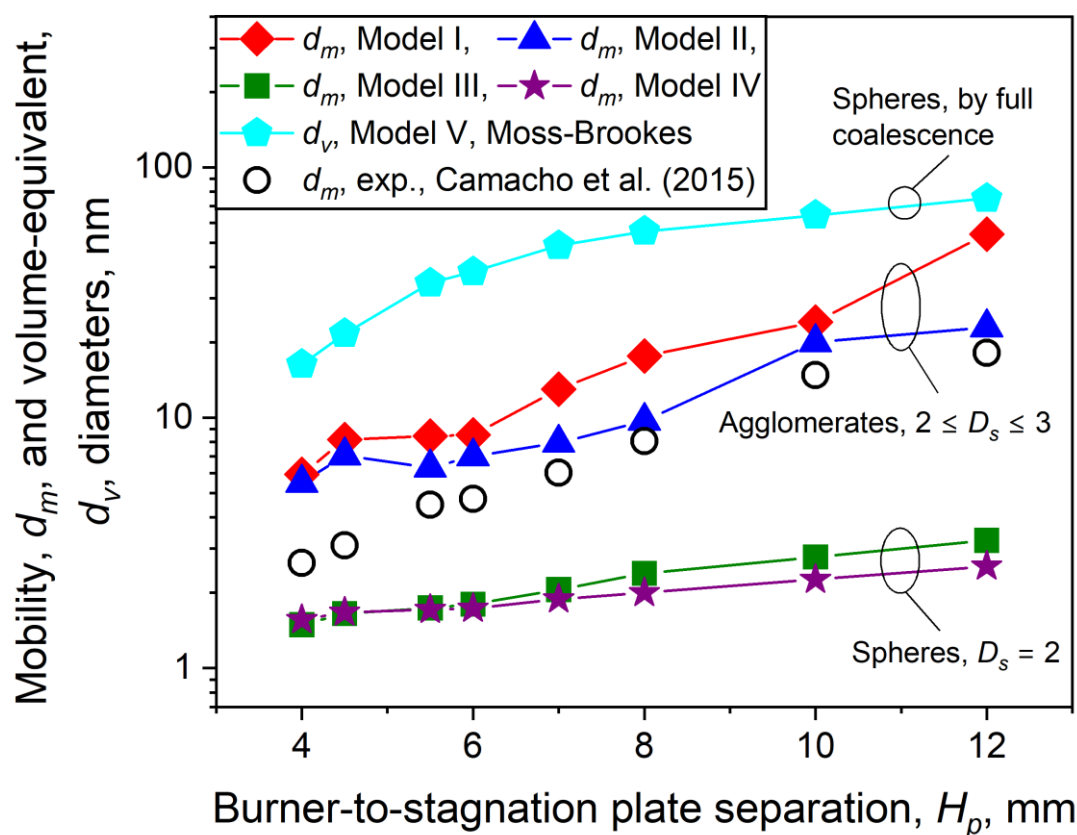280   chemistry or the assumption of a non-variable density for nascent soot (Hou et al., 2019).

Figure 7: Soot mobility diameter (d_m) predicted by the CFD-coupled monodisperse PD framework (Models I–IV) and volume-equivalent diameter (d_v) predicted by the Moss-Brookes soot model (Model V; full coalescence) (filled symbols). The model predictions are compared to the average d_m from SMPS measurements in premixed ethylene flames (Camacho et al., 2015).

285

Figure 7 shows the soot mobility diameter, d_m, predicted by Models I–IV using the CFD-coupled monodisperse PD framework developed in this study. The volume-equivalent diameter, d_v, is also shown as predicted by the Moss-Brookes soot model (Model V), which assumes coagulation by full coalescence neglecting the formation of particles with fractal-like structure (i.e., $d_p = d_m = d_v$). The model predictions are compared with the average d_m derived from particle size distributions measured

290   by the scanning mobility particle sizer (SMPS) in premixed ethylene flames (Camacho et al., 2015). All monodisperse models capture the expected increase in particle size with increasing burner-to-stagnation plate separation. The MD-informed nucleation model (Model II) shows the best agreement with the measured mobility diameters, esp. for $H_p \geq 6$ mm, followed by the baseline Model I, which predicts slightly larger diameters at all H_p. Both Models I and II predict the formation of fractal-like agglomerates (as shown in Fig. S2 for Model II) with $2 \leq D_s \leq 3$, capturing the fractal-like morphology of soot aggregates

295   produced in flames. Models III and IV, which employ the MD-derived surface growth rate, suggest limited particle growth (< 3 nm) and nearly spherical particle formation ($D_s = 2$, based on the D_s correlation used in Fakharnezhad et al. (Fakharnezhad et al., 2026)) even at large separation distances ($H_p \geq 8$ mm). In contrast, Model V overestimates particle size substantially due to the much higher carbon addition during surface growth compared to HACA-based or MD-derived correlations. This model inherently predicts spherical particles, as it explicitly assumes coagulation by full coalescence (Brookes and Moss, 1999).

300   The baseline framework (Model I), accounting for the semi-empirical nucleation rate and the HACA surface growth rate, captures the overall trend of the soot number density (Fig. 6a), volume fraction (Fig. 6b), and particle size (Fig. 7). Accounting for the MD-derived nucleation rate, Model II improves the f_v and d_m predictions, nicely matching the soot volume fraction and SMPS measurements in this flame, and even predicts comparable N (within one order of magnitude) with the detailed sectional model across all H_p. It should be noted that even though the lumped MD-derived nucleation rate employed

305   in Model II cannot capture the level of chemical detail accounted for in sectional models interfaced with chemical kinetic reaction mechanisms, it does capture f_v and d_m measurements with reasonable accuracy at significantly lower computational cost.

4 Conclusions

A multiscale modeling framework was developed that couples a monodisperse particle dynamics (PD) model with

310   computational fluid dynamics (CFD) describing soot formation and growth in a premixed ethylene burner-stabilized stagnation (BSS) flame. The coupled PD-CFD model, accounting for simultaneous nucleation, surface growth, and coagulation, is used to evaluate the effect of nucleation and surface growth rate equations developed semi-empirically or by molecular dynamics (MD) on the soot number density, volume fraction, and soot mobility diameter. Accounting for the semi-empirical Moss-Brookes nucleation rate and the Hydrogen Abstraction Carbon Addition (HACA) surface growth rate (Model I, baseline),

315   reproduces the soot number density, volume fraction, and particle size measurements reasonably well across the BSS flame. Incorporating the MD-derived nucleation rate and the HACA surface growth model (Model II) further improved soot volume

fraction and mobility diameter predictions compared to those obtained by semi-empirical rates, nicely matching measurements and a sectional model with detailed chemical kinetic mechanism (Saggese et al., 2015) in the post-flame region ($H_p \geq 6$ mm). Model II, encompassing the MD-informed nucleation rate, reproduced mobility diameter measurements most accurately

320 among all reduced models and yielded soot volume fractions within one order of magnitude from experimental data, outperforming reduced models employing the MD-derived or Moss-Brookes surface growth rate. Even though the developed MD-informed CFD-PD framework does not include the detail accounted for in chemical kinetic mechanisms, it captures the measured f_v and d_m reasonably well, resulting in even comparable predictions to those by a detailed sectional model in the post-nucleation flame region, at significantly lower computational cost. This framework provides a promising foundation for

325 predictive, design-oriented simulations of combustion and aerosol synthesis systems.

Supplementary Information

Figures showing the variation of carbon addition rate due to surface growth as a function of height above the burner, and the evolution of soot particle sizes (primary and mobility diameters) with burner-to-stagnation plate separation.

Author contributions

330 AF: writing (original draft), visualization, validation, software, methodology, formal analysis, data curation, conceptualization. JDB: writing (review and editing), methodology, supervision. EG: writing (review and editing), supervision, software, resources, methodology, conceptualization.

Competing interests

One of the (co-)authors is a member of the editorial board of *Aerosol Research.* The authors declare that they have no other

335 competing interests.

Acknowledgements

References

340 Appel, J., Bockhorn, H., and Frenklach, M.: Kinetic modeling of soot formation with detailed chemistry and physics: laminar premixed flames of C2 hydrocarbons, Combustion and Flame, 121, 122–136, https://doi.org/10.1016/S0010-2180(99)00135-2, 2000.

Brookes, S. J. and Moss, J. B.: Predictions of soot and thermal radiation properties in confined turbulent jet diffusion flames, Combustion and Flame, 116, 486–503, Doi 10.1016/S0010-2180(98)00056-X, 1999.

345   Buesser, B., Grohn, A. J., and Pratsinis, S. E.: Sintering Rate and Mechanism of TiO(2) Nanoparticles by Molecular Dynamics, J Phys Chem C Nanomater Interfaces, 115, 11030–11035, 10.1021/jp2032302, 2011.

Camacho, J., Liu, C., Gu, C., Lin, H., Huang, Z., Tang, Q., You, X., Saggese, C., Li, Y., Jung, H., Deng, L., Wlokas, I., and Wang, H.: Mobility size and mass of nascent soot particles in a benchmark premixed ethylene flame, Combustion and Flame, 162, 3810–3822, https://doi.org/10.1016/j.combustflame.2015.07.018, 2015.

350   Chen, B., Liu, D., and Liu, M.: Combining Langevin dynamics and CFD-PBM model to predict TiO2 nanoparticle evolution during aerosol synthesis, Applied Thermal Engineering, 230, 10.1016/j.applthermaleng.2023.120702, 2023.

Chen, D. and Luo, K. H.: Reactive sites on the surface of polycyclic aromatic hydrocarbon clusters: A numerical study, Combustion and Flame, 211, 362–373, 10.1016/j.combustflame.2019.09.034, 2020.

Fakharnezhad, A., Kelesidis, G. A., Berry, J. D., and Goudeli, E.: Nucleation, surface growth and coagulation of soot by
355   hierarchical modeling, Powder Technology, 469, 10.1016/j.powtec.2025.121747, 2026.

Fakharnezhad, A., Saad, D. M., Kelesidis, G. A., and Goudeli, E.: Nucleation rate of carbonaceous nanoparticles by n-heptane pyrolysis at high pressure and temperature via molecular dynamics simulations, Aerosol Science and Technology, 59, 1137–1150, 10.1080/02786826.2025.2480625, 2025.

Frenklach, M.: Reaction mechanism of soot formation in flames, Physical Chemistry Chemical Physics, 4, 2028–2037,
360   10.1039/b110045a, 2002.

Gerasimov, I. E., Knyazkov, D. A., Yakimov, S. A., Bolshova, T. A., Shmakov, A. G., and Korobeinichev, O. P.: Structure of atmospheric-pressure fuel-rich premixed ethylene flame with and without ethanol, Combustion and Flame, 159, 1840–1850, https://doi.org/10.1016/j.combustflame.2011.12.022, 2012.

Goudeli, E.: Nanoparticle growth, coalescence, and phase change in the gas-phase by molecular dynamics, Current Opinion
365   in Chemical Engineering, 23, 155–163, 10.1016/j.coche.2019.04.001, 2019.

Goudeli, E., Eggersdorfer, M. L., and Pratsinis, S. E.: Coagulation-agglomeration of fractal-like particles: structure and self-preserving size distribution, Langmuir, 31, 1320–1327, 10.1021/la504296z, 2015.

Goudeli, E., Eggersdorfer, M. L., and Pratsinis, S. E.: Coagulation of Agglomerates Consisting of Polydisperse Primary Particles, Langmuir, 32, 9276–9285, 10.1021/acs.langmuir.6b02455, 2016.

370   Goudeli, E., Ganguly, A., Kelesidis, G. A., Fakharnezhad, A., and Roy, S. P.: Surface growth rate of soot by reactive Molecular Dynamics (under review), 2025.

Harris, S. J. and Weiner, A. M.: Chemical-Kinetics of Soot Particle Growth, Annual Review of Physical Chemistry, 36, 31–52, DOI 10.1146/annurev.physchem.36.1.31, 1985.

Hou, D., Lindberg, C. S., Manuputty, M. Y., You, X., and Kraft, M.: Modelling soot formation in a benchmark ethylene
375   stagnation flame with a new detailed population balance model, Combustion and Flame, 203, 56–71, 10.1016/j.combustflame.2019.01.035, 2019.

Hulburt, H. M. and Katz, S.: Some problems in particle technology: A statistical mechanical formulation, Chemical Engineering Science, 19, 555–574, https://doi.org/10.1016/0009-2509(64)85047-8, 1964.

380 Johnson, P. R., Chakrabarty, R. K., and Kumfer, B. M.: A modeling approach for soot formation in non-premixed flames with elevated stoichiometric mixture fraction, Combustion and Flame, 229, 111383, https://doi.org/10.1016/j.combustflame.2021.02.029, 2021.

Kazakov, A. and Frenklach, M.: Reduced Reaction Sets based on GRI-Mech 1.2 (DRM19 and DRM22), University of California, Berkeley [code], 1995.

Kee, R. J., Coltrin, M. E., and Glarborg, P.: Chemically reacting flow: theory and practice, John Wiley & Sons2005.

385 Kelesidis, G. A. and Goudeli, E.: Self-preserving size distribution and collision frequency of flame-made nanoparticles in the transition regime, Proceedings of the Combustion Institute, 38, 1233–1240, 10.1016/j.proci.2020.07.147, 2021.

Kelesidis, G. A., Goudeli, E., and Pratsinis, S. E.: Flame synthesis of functional nanostructured materials and devices: Surface growth and aggregation, Proceedings of the Combustion Institute, 36, 29–50, https://doi.org/10.1016/j.proci.2016.08.078, 2017.

390 Kholghy, M. R. and Kelesidis, G. A.: Surface growth, coagulation and oxidation of soot by a monodisperse population balance model, Combustion and Flame, 227, 456–463, https://doi.org/10.1016/j.combustflame.2021.01.010, 2021.

Kholghy, M. R., Kelesidis, G. A., and Pratsinis, S. E.: Reactive polycyclic aromatic hydrocarbon dimerization drives soot nucleation, Phys Chem Chem Phys, 20, 10926–10938, 10.1039/c7cp07803j, 2018.

Kruis, F. E., Kusters, K. A., Pratsinis, S. E., and Scarlett, B.: A Simple Model for the Evolution of the Characteristics of 395 Aggregate Particles Undergoing Coagulation and Sintering, Aerosol Science and Technology, 19, 514–526, 10.1080/02786829308959656, 1993.

Mao, Q., van Duin, A. C. T., and Luo, K. H.: Formation of incipient soot particles from polycyclic aromatic hydrocarbons: A ReaxFF molecular dynamics study, Carbon, 121, 380–388, 10.1016/j.carbon.2017.06.009, 2017.

Michelsen, H. A.: Probing soot formation, chemical and physical evolution, and oxidation: A review of in situ diagnostic 400 techniques and needs, Proceedings of the Combustion Institute, 36, 717–735, https://doi.org/10.1016/j.proci.2016.08.027, 2017.

Mitchell, P. and Frenklach, M.: Particle aggregation with simultaneous surface growth, Physical Review E, 67, 061407, 10.1103/PhysRevE.67.061407, 2003.

Patterson, R. I. A. and Kraft, M.: Models for the aggregate structure of soot particles, Combustion and Flame, 151, 405 10.1016/j.combustflame.2007.04.012, 2007.

Ranzi, E., Frassoldati, A., Grana, R., Cuoci, A., Faravelli, T., Kelley, A. P., and Law, C. K.: Hierarchical and comparative kinetic modeling of laminar flame speeds of hydrocarbon and oxygenated fuels, Progress in Energy and Combustion Science, 38, 468–501, https://doi.org/10.1016/j.pecs.2012.03.004, 2012.

Saggese, C., Cuoci, A., Frassoldati, A., Ferrario, S., Camacho, J., Wang, H., and Faravelli, T.: Probe effects in soot sampling 410 from a burner-stabilized stagnation flame, Combustion and Flame, 167, 184–197, 10.1016/j.combustflame.2016.02.013, 2016.

Saggese, C., Ferrario, S., Camacho, J., Cuoci, A., Frassoldati, A., Ranzi, E., Wang, H., and Faravelli, T.: Kinetic modeling of particle size distribution of soot in a premixed burner-stabilized stagnation ethylene flame, Combustion and Flame, 162, 3356–3369, 10.1016/j.combustflame.2015.06.002, 2015.

415 Schulz, F., Commodo, M., Kaiser, K., De Falco, G., Minutolo, P., Meyer, G., D'Anna, A., and Gross, L.: Insights into incipient soot formation by atomic force microscopy, Proceedings of the Combustion Institute, 37, 885–892, 10.1016/j.proci.2018.06.100, 2019.

Sharma, A., Mukut, K. M., Roy, S. P., and Goudeli, E.: The coalescence of incipient soot clusters, Carbon, 180, 215–225, 10.1016/j.carbon.2021.04.065, 2021.

Trivanovic, U. and Pratsinis, S. E.: Opinion: Eliminating aircraft soot emissions, Aerosol Research, 2, 207–223, 10.5194/ar-420 2-207-2024, 2024.

Xiong, Y. and Pratsinis, S. E.: Formation of agglomerate particles by coagulation and sintering—Part I. A two-dimensional solution of the population balance equation, Journal of Aerosol Science, 24, 10.1016/0021-8502(93)90003-R, 1993.